Constraining the QCD phase diagram

Owe Philipsen[1]

[1]Institute for Theoretical Physics, Goethe University Frankfurt,
Max-von-Laue-Str. 1, D-60438 Frankfurt am Main, Germany

Abstract. Lattice QCD and functional methods are making significant progress in constraining the QCD phase diagram. As an important milestone, the chiral phase transition with massless u, d-quarks at zero density is now understood to be of second order for all strange quark masses, and a smooth crossover as soon as $m_{u,d} \neq 0$. Together with information on fluctuations and refined reweighted simulations, this bounds a possible critical point to be at $\mu_B/T \gtrsim 3$. On the other hand, an approximately chiral-spin symmetric temperature window has been discovered above the chiral crossover, $T_{\rm ch} \lesssim T \lesssim 3T_{\rm ch}$, with distinct correlator multiplet patterns and a pion spectral function suggesting resonance-like degrees of freedom, which dissolve gradually with temperature.

1 Introduction

Knowledge of the QCD phase diagram is of great importance for the physics of heavy ion collisions and neutron stars. Theoretical predictions from lattice QCD are severely hampered by a fermion sign problem, which prohibits straightforward Monte Carlo simulations at finite baryon chemical potential. Nevertheless, methods working for $\mu_B \lesssim 3T$ as well as studies of the general parameter dependence of the chiral phase transition have reached a new level of maturity, providing phenomenologically relevant constraints on the location of a possible critical point.

The expected scenario for physical QCD is intimately connected to the situation in the chiral limit of massless u, d-quarks [1–3], as sketched in Fig. 1. For $m_{u,d} = 0$ there is an exact chiral symmetry, whose breaking/restoration across $T_c(\mu_B)$ must proceed by a non-analytic phase transition. If this transition is second-order at $\mu_B = 0$ and first-order at $T = 0$, as in several low-energy models, there must be a tricritical point where the order of the transition changes. On quite general grounds, a $Z(2)$-critical line emanates from a tricritical point in in the direction of the symmetry breaking field (i.e. $m_{u,d}$), with a known tricritical exponent [4], and represents the critical endpoint at physical mass values. However, if nothing is known about the chiral limit, other possibilities are transition lines that are entirely first or entirely second order for $m_{u,d} = 0$, and the situation at physical masses would be different. This illustrates the importance of the chiral limit to both constrain and understand the physical phase diagram.

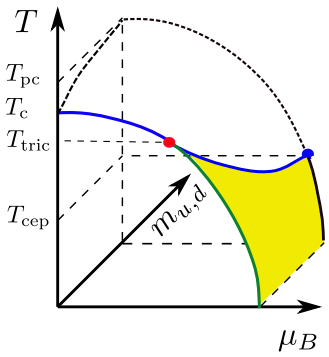

Figure 1. Connection of the putative QCD phase diagram for physical light quark masses to the chiral limit in the front plane.

2 The chiral transition at $\mu_B = 0$

In the chiral limit the quark determinant in the partition function diverges, prohibiting direct simulations and making its approach computationally expensive. For decades expectations have thus been based on an analysis of 3d sigma models as low energy effective theories, augmented by a 't Hooft term for the $U(1)_A$ anomaly, whose renormalisation group flow based on the epsilon expansion [5] predicts the chiral phase transition to be first-order for $N_f \geq 3$. The case of $N_f = 2$ was found to crucially depend on the anomalous $U(1)_A$ symmetry: If it remains broken at T_c, the chiral transition should be second order in the $O(4)$-universality class, whereas its effective restoration would enlarge the symmetry and push the transition to first order.

Early QCD simulations on coarse lattices were consistent with the scenario shown in Fig. 2 (left): A first-order region could be seen for $N_f = 3$, whereas the smallest available masses showed a continuous crossover for $N_f = 2$. However, the location of the $Z(2)$-boundary varies widely between different discretisations, indicating large cutoff effects. The general pattern is for the first-order region to shrink when the lattice is made finer, while improved staggered actions see no trace of a first-order transition at all. For a more detailed discussion and list of references see [7].

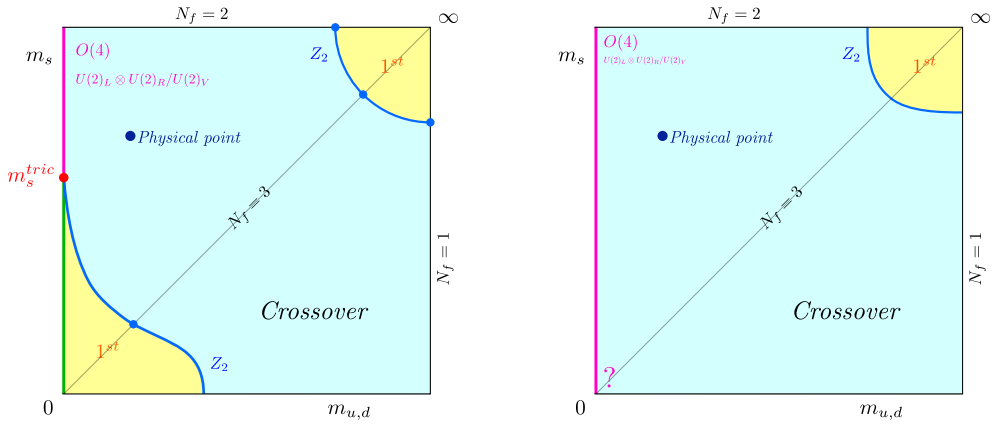

Figure 2. The order of the QCD thermal transition as a function of the quark masses. Left: Scenario proposed in [5] and observed on coarse lattices. Right: Emerging continuum limit [6]. The universality class in the three-flavour chiral limit is not yet known. From [6].

Recent investigations using the Highly Improved Staggered Quark (HISQ) action start at the $N_f = 2 + 1$ physical point and then gradually reduce the light quark mass until $m_{PS} \approx 55$ MeV [8]. Fig. 3 (left) shows the chiral susceptibility normalised to its peak value at the physical pion mass. The peak location defines the pseudo-critical temperature T_{pc}. However, the peak height stays finite and no sign of a first-order transition is detectable. Analytic fRG calculations in infinite volume [9] are compatible with this behaviour, Fig. 3 (left). Similar results are found using twisted mass Wilson fermions at quark masses at and above the physical point [10]. Thus either a $Z(2)$-critical point bounding a very narrow first-order region is approached, or a second-order transition in the chiral limit.

Eventually one would like to calculate the critical exponents characterising the approach to criticality, and thus determine the universality class from first principles. However, this requires exponential accuracy in the numerically expensive light mass regime and is not feasible. In practice the data are fitted to scaling formulae with exponents fixed to known values for the universality classes in question, such as the approach of the crossover temperature to the critical temperature T_c in the chiral limit,

$$T_{pc}(m_l) = T_c\left(1 + K\, m_l^{1/\beta\delta}\right) + \text{sub-leading}\,. \qquad (1)$$

The extrapolated chiral critical temperatures are

$$\begin{aligned} T_c &= 132^{+3}_{+6}\ \text{MeV} \quad \text{HISQ fermions [8]}\,, \\ T_c &= 134^{+6}_{-4}\ \text{MeV} \quad \text{twisted mass Wilson [10]}\,, \\ T_c &= 142^{+0.5}_{-0.5}\ \text{MeV} \quad \text{fRG methods [9]}\,. \end{aligned}$$

The variation between the possible sets of critical exponents is covered by the errors, so that an extrapolation makes sense even without definite knowledge of the true universality class.

A first-order chiral transition for $N_f \in [2, 7]$ could recently be practically ruled out by investigating the effects of the number of flavours, their masses and the lattice spacing [6] on the transition. The study exploits the fact that a change from a first-order to a second-order chiral transition necessarily passes through a tricritical point, such as in the scenario Fig. 2 (left). This implies tricritical scaling with known exponents for the $Z(2)$ boundary line as it approaches the chiral limit, allowing for a controlled extrapolation. Rather than varying quark masses independently, ref. [6] continuously varies the number N_f of degenerate quarks [12]. A tricritical m_s^{tric} as in Fig. 2 (left) then translates into a tricritical $2 < N_f^{\text{tric}} < 3$. On the lattice, such a tricritical point additionally depends on the lattice spacing, $N_f^{\text{tric}}(a)$, which can be inverted to $a^{\text{tric}}(N_f)$.

Fig. 3 (middle) shows the $Z(2)$-critical boundary line separating the light bare quark mass region featuring first-order transitions from the crossover region as a function of lattice spacing for the unimproved staggered fermion action. In agreement with previous studies, the first-order region grows as more flavours are added, and it shrinks as the lattice is made finer. Those N_f-theories with three available lattice spacings show tricritical scaling and a tricritical point in the lattice chiral limit, which is moving to the left as N_f is increased. Note that the continuum limit is in the origin at $(am, aT) = (0, 0)$. This implies a tricritical point in the continuum limit to be beyond $N_f^{\text{tric}} > 7$. Conversely, the first-order regions observed in these simulations are *not* connected to the continuum limit and must be regarded as lattice artefacts. A powerful check on this finding is provided by $N_f = 3$ $O(a)$-improved Wilson fermions [11]. Plotting those data in terms of the appropriate scaling variable, perfect tricritical scaling is observed, Fig. 3 (right), so that the continuum transition is of second order as in the staggered case. Two further discretisations with $N_f = 3$, HISQ fermions [13] and domain wall fermions [14], do not see any phase transition at the smallest available quark masses, and thus are fully consistetnt with those findings. A recent fRG study of 3d sigma models including a ϕ^6 term [15] and numerical bootstrap methods applied to $U(m)\times U(n)$ [16] models are also compatible with a second-order chiral transition. Thus, the Columbia plot in the continuum looks as in Fig. 2 (right), with a second-order chiral transition for $m_{u,d} = 0$ and any value of m_s, and crossover as soon as $m_{u,d} \neq 0$.

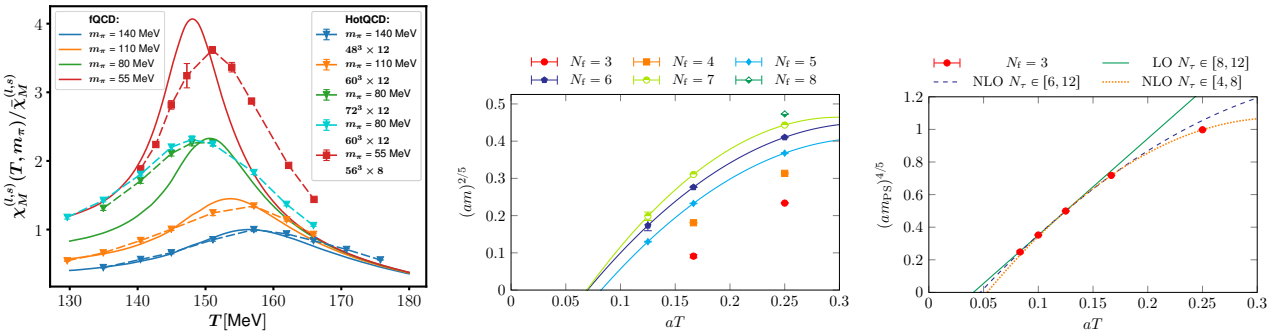

Figure 3. Left: Chiral susceptibility at physical m_s for a range of decreasing $m_{u,d}$ with the HISQ lattice action [8] and from fRG calculations [9]. From [9]. The $Z(2)$-critical line separating first-order transitions (below) from crossover (above), for unimproved staggered fermions [6] (middle) and $O(a)$-improved Wilson fermions [11] (right), with tricritical scaling fits to both. From [6].

3 The search for a critical point

Lattice searches for a critical point are based on indirect methods to extract information about the phase structure for small baryon density, $\mu_B/T \lesssim 3$: (i) Reweighting [17], (ii) Taylor expansion in μ/T [18] and (iii) analytic continuation from imaginary chemical potential, for which there is no sign problem [19, 20]. When the QCD pressure is expressed as a series in baryon chemical potential,

$$\frac{p(T,\mu_B)}{T^4} = \frac{p(T,0)}{T^4} + \sum_{n=1}^{\infty} \frac{1}{2n!} \chi_{2n}^B(T) \left(\frac{\mu_B}{T}\right)^{2n}, \quad (2)$$

$$\chi_{2n}^B(T) = \frac{\partial^{2n}(\frac{p}{T^4})}{\partial(\frac{\mu_B}{T})^{2n}}\Big|_{\mu_B=0},$$

the Taylor coefficients are the baryon number fluctuations evaluated at zero density, which can also be computed by fitting to untruncated results at imaginary μ_B. This permits full control of the systematics between (ii) and (iii). These coefficients are presently known up to $2n = 8$.

Quite generally power series are limited by their radius of convergence, corresponding to the nearest singularity of the full function (relative to the expansion point) in the complex variable. If such a singularity is located on the real axis, it signals a phase transition.

In [21] a cluster expansion model (CEM) was developed, with all expansion coefficients recursively related to the lower ones, and the first two are fixed by lattice data. As in the virial expansion, such a recursion is possible as long as the system is sufficiently dilute and dominated by two-body interactions. The model is quantitatively consistent with all known lattice pressure coefficients, as e.g. in Fig. 4 (left), and since its coefficients are known to all orders, it allows a controlled extraction of the radius of convergence. The only phase transition predicted in this way is the known Roberge-Weiss transition in the direction of imaginary chemical potential $\mu_B = i\pi T$ [22], which implies that any phase transition in the real direction is further away than that. While this is just a model, it tells us that nothing in the available lattice fluctuation data enforces singular behaviour.

Another option is to use the coefficients calculated directly from the lattice. From these one can construct Padé-approximants, which are rational functions (i.e. infinite order in the expansion variable) whose first coefficients agree with the explicitly computed ones. These approximants can be further constrained by simulation results for the full pressure at imaginary chemical potential. Their singularities are then taken as estimates for the singularities of the full function. Locations of the Lee-Yang edge singularities (indicating a branch point in the pressure) extracted in this way are shown in Fig. 4 (middle), based on HISQ fermion data [23]. So far all singularities are at complex values of the chemical potential, but note the closing in toward the real axis as temprerature is decreased. This bounds a true phase transition to lower temperatures than those for which coefficients are currently available.

Table 1. Lattice bounds on the location of a critical point

Criterion	$(\mu_B/T)^{\rm cep} \gtrsim$	Ref.
$T_{\rm cep} < T_c$ as in Fig. 1	3.1	[7]
CEM of lattice fluctuations	π	[21]
Padé-appr. LY-zeroes	2.5	[23]
Reweighted simulation	2.5	[24]

Taylor expansions are avoided by using reweighting techniques in Monte Carlo simulations. Recent new calculations with stout smeared staggered fermions [24], using techniques considerably refined compared to earlier ones, evaluate the renormalised chiral condensate,

$$\langle\bar{\psi}\psi\rangle_R(T,\mu) = -\frac{m_{ud}}{f_\pi^4}\left[\langle\bar{\psi}\psi\rangle_{T,\mu} - \langle\bar{\psi}\psi\rangle_{0,0}\right], \quad (3)$$

as shown in Fig. 4 (right). The reweighted real μ_B simulations are fully compatible with the analytic continuation from imaginary μ_B simulations, but with smaller errors. Neither method shows a sign of non-analyticity so far.

In summary, lattice information on physical QCD in equilibrium at $\mu_B/T \leq 3$ is increasing and increasingly controlled. Table 1 collects the current bounds on the location of a critical endpoint resulting from these analyses. These are also consistent with the critical endpoint candidates found in the most recent truncations of Dyson-Schwinger equations [26] and their combination with functional renormalisation group methods [27], which predict $(\mu_B/T)^{\rm cep} \approx 5.6$.

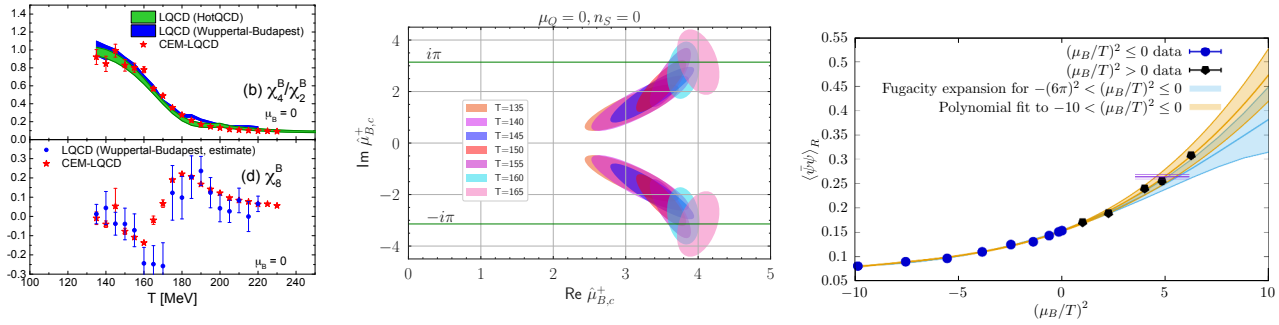

Figure 4. Left: Baryon number fluctuations from the lattice in comparison with the CEM model. From [25]. Middle: Lee-Yang zeros indicating the radius of convergence of the pressure series in complex chemical potential. From [23]. Right: Renormalised chiral condensate as a function of real and imaginary chemical potential. From [24].

4 Emergent chiral spin symmetry

While a critical point remains elusive on the lattice so far, an emergent approximate chiral spin symmetry has been discovered above the chiral crossover at $\mu_B = 0$. A $SU(2)_{CS}$ chiral spin transformation acts on Dirac fields as

$$\psi(x) \to \exp\left(i\vec{\Sigma}\cdot\vec{\epsilon}\right)\psi(x)\,, \quad \vec{\Sigma} = (\gamma_k, -i\gamma_5\gamma_k, \gamma_5)\,. \tag{4}$$

Here $k = 1,\ldots 4$ can be any of the euclidean gamma matrices. From the generators it is apparent that $SU(2)_{CS} \supset U(1)_A$. When combined with ordinary vectorial isospin transformations, $SU(2)_{CS} \otimes SU(2)_V$ can be embedded into the larger $SU(4)$, which contains the usual chiral symmetry of the massless QCD Lagrangian, $SU(4) \supset SU(2)_L \times SU(2)_R \times U(1)_A$.

The QCD Lagrangian is not invariant under chiral spin transformations. A thermal medium implies a preferred Lorentz frame, and the massless quark action can be decomposed as

$$\bar{\psi}\gamma_\mu D_\mu\psi = \bar{\psi}\gamma_0 D_0\psi + \bar{\psi}\gamma_i D_i\psi\,. \tag{5}$$

Explicit calculation shows the colour-electric part of the quark-gluon interaction to be CS- and $SU(4)$-invariant, while the colour-magnetic interaction and kinetic terms (and thus the free Dirac action) are not. Hence, chiral spin symmetry is never exact in physical QCD, but its approximate realisation is possible if the colour-electric quark-gluon interaction dominates the quantum effective action in some dynamical range, which would then be strongly coupled.

On the lattice, symmetries become apparent in degeneracy patterns of euclidean correlation functions,

$$C_\Gamma(\tau,\mathbf{x}) = \langle O_\Gamma(\tau,\mathbf{x})\, O_\Gamma^\dagger(0,\mathbf{0})\rangle\,, \tag{6}$$

with Γ some appropriate Dirac matrix. Information about all excitations in each quantum number channel is carried by the spectral functions $\rho_\Gamma(\omega,\mathbf{p})$,

$$C_\Gamma(\tau,\mathbf{p}) = \int_0^\infty \frac{d\omega}{2\pi}\, K(\tau,\omega)\rho_\Gamma(\omega,\mathbf{p})\,, \tag{7}$$
$$K(\tau,\omega) = \frac{\cosh(\omega(\tau-1/2T))}{\sinh(\omega/2T)}\,.$$

For an isotropic system in equilibrium, it is sufficient to probe the spatial and temporal correlators averaged over the orthogonal directions,

$$C_\Gamma^s(z) = \sum_{x,y,\tau} C_\Gamma(\tau,\mathbf{x})\,, \quad C_\Gamma^\tau(\tau) = \sum_{x,y,z} C_\Gamma(\tau,\mathbf{x})\,. \tag{8}$$

Numerical results for spatial $J = 0, 1$ meson correlators from $N_f = 2$ JLQCD domain wall fermions with physical quark masses, good chiral symmetry and lattice spacings < 0.1 fm [28] are shown in Fig. 5. Three multiplets of spatial correlators, $E_{1,2,3}$, at different temperatures are seen. Of these, E_1 is due to $U(1)_A$ restoration whereas E_3 requires the full chiral symmetry. Both multiplets are expected above the chiral crossover. Not expected is the multiplet E_2, which does *not* correspond to a representation of chiral symmetry, but to one of the larger $SU(4)$. For the representations and associated meson states, see [29, 30]. Appearance of E_2 demonstrates the dynamical emergence of chiral spin symmetry in this regime. As temperature is further increased, E_2 gradually disappears as a separate multiplet and only those belonging to the expected chiral symmetry survive. Similar findings are reported from temporal correlators at $T = 220$ MeV and the same lattice spacing [31]. Recently, the same patterns were observed with the quark content increased to $N_f = 2 + 1 + 1$ QCD, including physical strange and charm quarks [32].

A related observable which is sensitive to the entry and exit of the CS-symmetric temperature range are screening masses [33]. These correspond to the exponential decay of the large-separation spatial correlators in (8), $C_\Gamma^s(z) \sim \exp(-m_{scr}z)$ for $z \to \infty$. While not directly accessible experimentally, they can be readily evaluated non-perturbatively and perturbatively. Around the chiral crossover temperature, the screening masses show the expected degeneracy due to chiral symmetry. However, the temperature dependence predicted by pertubation theory is only attained for $T \gtrsim 500$ MeV. This can be understood by the approximate chiral spin symmetry in between, which perturbation theory about free quarks cannot reproduce.

If there is a chiral-spin symmetric band at zero density, it must necessarily continue to finite baryon density because the μ_B-term respects that symmetry. From the known behaviour of screening masses with μ_B one

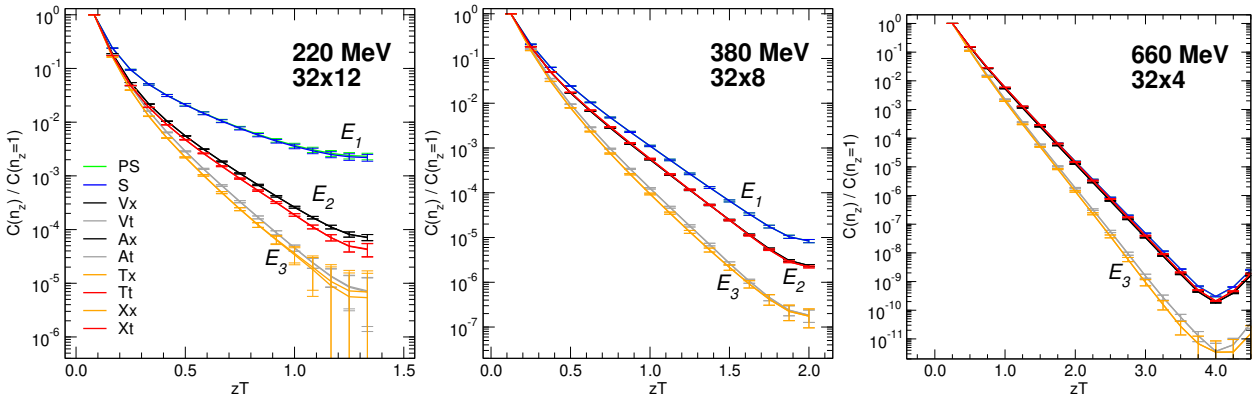

Figure 5. Spatial correlation functions with domain wall fermions show distinct E_1, E_2, E_3 multiplets of the approximate $SU(4)$ chiral spin symmetry, at temperatures above the crossover. At large temperatures, these reduce to the multiplets of the ordinary chiral symmetry. From [28].

infers that the chiral-spin symmetric band curves downwards, as in the possible phase diagram Fig. 6 (left). In the absence of lattice data the continuation to higher densities and lower temperatures is speculative, of course, but baryon parity doublets and quarkyonic matter both are CS-symmetric candidates to populate such a band [33].

Information about the nature of the effective degrees of freedom in different regimes is encoded in the spectral functions, Eq. (8). Unfortunately, their extraction from discrete sets of lattice correlator data represents an ill-posed inversion problem. Recently, a new method was attempted [34], which applies to stable scalar particles in a heat bath, i.e. to the pion in the case of QCD, which allows to circumvent the integral inversion.

The method exploits locality of quantum field theories to ensure a representation of the spectral function [35, 36],

$$\rho_{\rm PS}(\omega,\mathbf{p}) \qquad (9)$$
$$= \int_0^\infty ds \int \frac{d^3u}{(2\pi)^2}\,\epsilon(p_0)\,\delta\big(\omega^2-(\mathbf{p}-\mathbf{u})^2-s\big)\,\widetilde{D}_\beta(\mathbf{u},s)\,,$$

with $\beta = 1/T$, the thermal spectral density $\widetilde{D}_\beta(\mathbf{u}, s)$, and the standard Källen-Lehmann vacuum representation arising as $T \to 0$. For stable massive particles the analytic vacuum structure of the spectral density is preserved in the absence of a true phase transition. The authors therefore propose an ansatz with separable particle and scattering contributions,

$$\widetilde{D}_\beta(\mathbf{u},s) = \widetilde{D}_{m,\beta}(\mathbf{u})\,\delta(s-m^2) + \widetilde{D}_{c,\beta}(\mathbf{u},s)\,. \qquad (10)$$

In an isotropic medium the spatial correlators and the spectral density are then related by [34]

$$C^s_{PS}(z) = \frac{1}{2}\int_0^\infty ds \int_{|z|}^\infty dR\, e^{-R\sqrt{s}} D_\beta(R,s). \qquad (11)$$

For temperatures below the threshold to the scattering states the first term in Eq. (10) should dominate. Once the continuum part is neglected, the calculation is straightforward. First, spatial pion correlators from [28] are fitted by the sum of two exponentials representing the π, π^*. This provides the $D_{m,\beta}(|\mathbf{x}|) = \alpha_{\pi,\pi^*}\exp(-\gamma_{\pi,\pi^*}|\mathbf{x}|)$, from which the spectral function can be reconstructed using Eqs. (9,10) and the known vacuum masses m_π, m_{π^*}. The result is shown in Fig. 6 (middle) and, as a non-trivial check, correctly predicts the temporal lattice correlator [31] for $\tau > m_{\pi^*}^{-1}$, Fig. 6 (right). The spectral function shows resonance-like peaks for both the pion and its first excitation. As the temperature increases, the peaks widen and gradually disappear, consistent with sequential hadron melting, but at temperatures significantly above the chiral crossover. This suggests non-perturbative, hadron-like excitations within the approximately chiral-spin symmetric temperature range.

5 Conclusions

The last few years have seen remarkable progress in the determination of the QCD phase structure. A major milestone is the understanding of the chiral transition at zero density in the massless limit, which is nearly completed. The transition temperature is known fairly accurately and there is strong evidence for the transition to be of second order for all $N_f \in [2, 7]$. Together with data on baryon number fluctuations, this constrains the location of a critical point to $(\mu_B/T)^{\rm cep} > 3$ and $T_{\rm cep} < 132$ MeV.

A new development is the discovery of an approximate chiral spin symmetry, which emerges dynamically in a temperature band above the chiral crossover, $T_{pc} \lesssim T \lesssim 3T_{pc}$. It can be identified in the multiplet structure of correlation functions and affects associated observables like screening masses and spectral functions. Together these suggest a regime with chiral symmetry restored but hadron-like degrees of freedom. It would be most interesting to investigate if and how this affects experimental observables in heavy ion collisions.

Acknowledgments: The author acknowledges support by the Deutsche Forschungsgemeinschaft (DFG) through the grant CRC-TR 211 “Strong-interaction matter under extreme conditions” and by the State of Hesse within the Research Cluster ELEMENTS (Project ID 500/10.006).

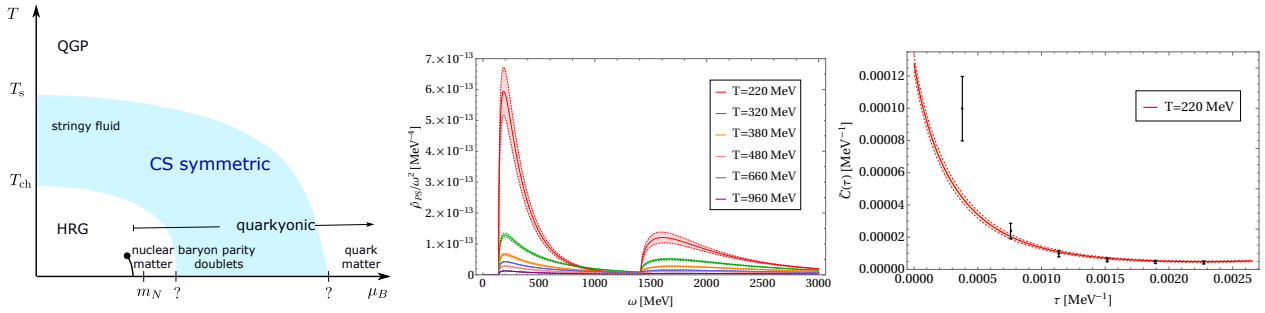

Figure 6. Left: a possible QCD phase diagram with a chiral-spin symmetric band. From [33]. Middle: Pion spectral function extracted from spatial lattice correlators. Right: Temporal correlator predicted by that spectral function, compared to lattice data. From [34].

References

[1] A.M. Halasz, A.D. Jackson, R.E. Shrock, M.A. Stephanov, J.J.M. Verbaarschot, Phys. Rev. D **58**, 096007 (1998), hep-ph/9804290

[2] K. Rajagopal, F. Wilczek, *The Condensed matter physics of QCD* (2000), pp. 2061–2151, hep-ph/0011333

[3] Y. Hatta, T. Ikeda, Phys. Rev. D **67**, 014028 (2003), hep-ph/0210284

[4] I. Lawrie, S. Sarbach, in *Phase transitions and critical phenomena*, edited by C. Domb, J. Lebowitz (1984), Vol. 9, p. 1

[5] R.D. Pisarski, F. Wilczek, Phys. Rev. D **29**, 338 (1984)

[6] F. Cuteri, O. Philipsen, A. Sciarra, JHEP **11**, 141 (2021), 2107.12739

[7] O. Philipsen, Symmetry **13**, 2079 (2021), 2111.03590

[8] H.T. Ding et al. (HotQCD), Phys. Rev. Lett. **123**, 062002 (2019), 1903.04801

[9] J. Braun, W.j. Fu, J.M. Pawlowski, F. Rennecke, D. Rosenblüh, S. Yin, Phys. Rev. D **102**, 056010 (2020), 2003.13112

[10] A.Y. Kotov, M.P. Lombardo, A. Trunin, Phys. Lett. B **823**, 136749 (2021), 2105.09842

[11] Y. Kuramashi, Y. Nakamura, H. Ohno, S. Takeda, Phys. Rev. D **101**, 054509 (2020), 2001.04398

[12] F. Cuteri, O. Philipsen, A. Sciarra, Phys. Rev. D **97**, 114511 (2018), 1711.05658

[13] L. Dini, P. Hegde, F. Karsch, A. Lahiri, C. Schmidt, S. Sharma, Phys. Rev. D **105**, 034510 (2022), 2111.12599

[14] Y. Zhang, Y. Aoki, S. Hashimoto, I. Kanamori, T. Kaneko, Y. Nakamura, PoS **LATTICE2022**, 197 (2023), 2212.10021

[15] G. Fejos, Phys. Rev. D **105**, L071506 (2022), 2201.07909

[16] S.R. Kousvos, A. Stergiou (2022), 2209.02837

[17] Z. Fodor, S.D. Katz, Phys. Lett. B **534**, 87 (2002), hep-lat/0104001

[18] C.R. Allton, S. Ejiri, S.J. Hands, O. Kaczmarek, F. Karsch, E. Laermann, C. Schmidt, L. Scorzato, Phys. Rev. D **66**, 074507 (2002), hep-lat/0204010

[19] P. de Forcrand, O. Philipsen, Nucl. Phys. B **642**, 290 (2002), hep-lat/0205016

[20] M. D'Elia, M.P. Lombardo, Phys. Rev. D **67**, 014505 (2003), hep-lat/0209146

[21] V. Vovchenko, J. Steinheimer, O. Philipsen, H. Stoecker, Phys. Rev. D **97**, 114030 (2018), 1711.01261

[22] A. Roberge, N. Weiss, Nucl. Phys. B **275**, 734 (1986)

[23] D. Bollweg, J. Goswami, O. Kaczmarek, F. Karsch, S. Mukherjee, P. Petreczky, C. Schmidt, P. Scior (HotQCD), Phys. Rev. D **105**, 074511 (2022), 2202.09184

[24] S. Borsanyi, Z. Fodor, M. Giordano, S.D. Katz, D. Nogradi, A. Pasztor, C.H. Wong, Phys. Rev. D **105**, L051506 (2022), 2108.09213

[25] V. Vovchenko, J. Steinheimer, O. Philipsen, A. Pasztor, Z. Fodor, S.D. Katz, H. Stoecker, Nucl. Phys. A **982**, 859 (2019), 1807.06472

[26] P.J. Gunkel, C.S. Fischer, Phys. Rev. D **104**, 054022 (2021), 2106.08356

[27] F. Gao, J.M. Pawlowski, Phys. Lett. B **820**, 136584 (2021), 2010.13705

[28] C. Rohrhofer, Y. Aoki, G. Cossu, H. Fukaya, C. Gattringer, L.Y. Glozman, S. Hashimoto, C.B. Lang, S. Prelovsek, Phys. Rev. D **100**, 014502 (2019), 1902.03191

[29] L.Y. Glozman, Eur. Phys. J. A **51**, 27 (2015), 1407.2798

[30] L.Y. Glozman, M. Pak, Phys. Rev. D **92**, 016001 (2015), 1504.02323

[31] C. Rohrhofer, Y. Aoki, L.Y. Glozman, S. Hashimoto, Phys. Lett. B **802**, 135245 (2020), 1909.00927

[32] T.W. Chiu (2023), 2302.06073

[33] L.Y. Glozman, O. Philipsen, R.D. Pisarski, Eur. Phys. J. A **58**, 247 (2022), 2204.05083

[34] P. Lowdon, O. Philipsen, JHEP **10**, 161 (2022), 2207.14718

[35] J. Bros, D. Buchholz, Nucl. Phys. B **429**, 291 (1994), hep-th/9807099

[36] J. Bros, D. Buchholz, Ann. Inst. H. Poincare Phys. Theor. **64**, 495 (1996), hep-th/9606046